NANO LETTERS

pubs.acs.org/NanoLett Letter

# Imaging Arrangements of Discrete Ions at Liquid–Solid Interfaces

Hao-Kun Li, J. Pedro de Souza, Ze Zhang, Joel Martis, Kyle Sendgikoski, John Cumings, Martin Z. Bazant, and Arun Majumdar*

Cite This: https://dx.doi.org/10.1021/acs.nanolett.0c02669 Read Online

ACCESS | Metrics & More | Article Recommendations | Supporting Information

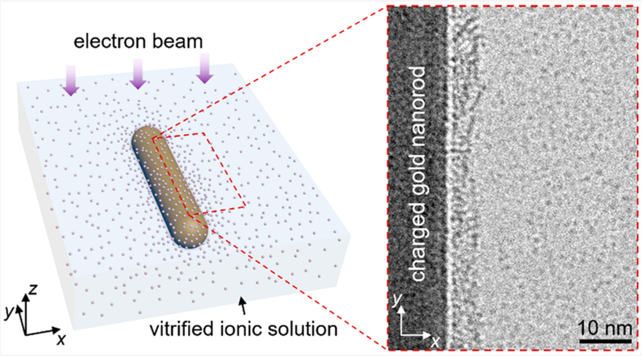

**ABSTRACT:** The individual and collective behavior of ions near electrically charged interfaces is foundational to a variety of electrochemical phenomena encountered in biology, energy, and the environment. While many theories have been developed to predict the interfacial arrangements of counterions, direct experimental observations and validations have remained elusive. Utilizing cryo-electron microscopy, here we directly visualize individual counterions and reveal their discrete interfacial layering. Comparison with simulations suggests the strong effects of finite ionic size and electrostatic interactions. We also uncover correlated ionic structures under extreme confinement, with the channel widths approaching the ionic diameter (∼1 nm). Our work reveals the roles of ionic size, valency, and confinement in determining the structures of liquid–solid interfaces and opens up new opportunities to study such systems at the single-ion level.

**KEYWORDS:** *electrical double layer, cryo-electron microscopy, single-ion imaging, ionic distribution*

Electrically charged liquid–solid interfaces are ubiquitous in nature and have been intensively studied over the last century.[1,2] The interplay between Coulombic interactions and the entropy of ions and solvent molecules determine ionic arrangements and distributions that typically span 1–100 nm in size. These interactions govern the behaviors of colloids and biomolecules,[3,4] the transport properties of biological and artificial membranes,[5−7] and the performance of various electrochemical systems such as supercapacitors,[8] batteries,[9,10] and catalysts.[11] At a fundamental level, the ionic distributions and the associated interfacial properties are controlled by both the discrete nature of individual ions and their collective interactions with (i) each other, (ii) the charged surface, and (iii) the surrounding medium. The ability to probe such systems with the single-ion resolution is, therefore, important to a basic understanding of their behaviors[12−17] and the development of new ionic technologies. There have been many attempts to probe liquid–solid interfaces using optical or X-ray spectroscopies,[18−23] but their spatial resolution remains inadequate to image discrete ions. Although scanning probe microscopy has been used to resolve ionic structures,[24−30] tip convolution and disturbance of the interface can make it difficult to interpret the observations.

In recent years, cryo-electron microscopy has been widely used in structural biology to examine biomolecules at the atomic scale.[31−34] Through rapid cooling, the native states of biomolecules are preserved in a thin layer of vitrified liquid and, therefore, can be observed inside electron microscopes. The utility of this technique beyond biology has enabled observation of a variety of interesting ionic phenomena under hydrated conditions, such as inorganic ligand monolayers,[35] host–guest chemistry,[36] and crystal formation.[37]

Here, for the first time, we implement cryo-electron microscopy to directly visualize individual counterions and their distributions at electrically charged liquid–solid interfaces (Figure 1a). We observe discrete layering of multivalent counterions, which stems from the finite ionic size and strong electrostatic interactions.[13−15,22,38−46] Moreover, correlated ionic structures under extreme confinement are revealed, with channel widths approaching the ionic diameter (∼1 nm). This technique offers new opportunities to investigate electrically charged liquid–solid interfaces at the single-ion level and provides a general mechanism to validate and improve computational and theoretical approaches.

Our samples were prepared by mixing amine-functionalized gold nanorods into aqueous solutions of phosphotungstic acid ($H_3PW_{12}O_{40}$) (ref 47). The nanorods are typically 20 nm in diameter and 120 nm in length (Figure S1). The Keggin anions ($[PW_{12}O_{40}]^{3-}$) contain multiple high-Z tungsten atoms, which strongly enhance the contrast in a transmission electron

**Received:** June 27, 2020
**Revised:** October 12, 2020

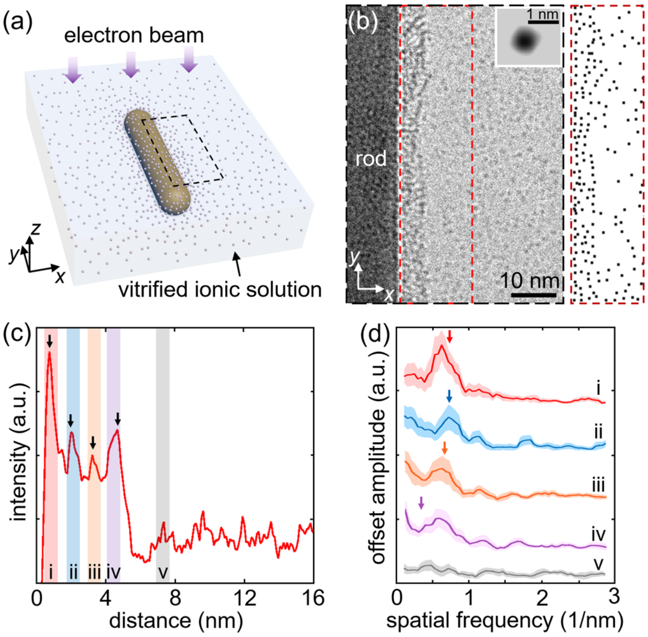

**Figure 1.** Cryo-TEM imaging of discrete ions and their distributions at the liquid−solid interface. (a) The sample consists of amine-functionalized gold nanorods embedded in an aqueous solution of phosphotungstic acid ($H_3PW_{12}O_{40}$). The amine functionalization groups are positively charged, which attract and redistribute the Keggin anions $[PW_{12}O_{40}]^{3-}$. A parallel electron beam is incident into the top surface ($+z$), and the exit wave produces a projected image in the ($x$−$y$) plane. (b) A typical cryo-TEM image of the interface between a nanorod and the electrolyte solution (dashed region in panel a). The image contrast in the electrolyte solution is dominated by the Keggin anions, which contain multiple high-Z tungsten atoms. The inset shows a noise-filtered image of a single Keggin anion in vitrified solution. The central positions of the high-intensity spots in the red region are marked on the right. (c) Integrated image intensity profile within 16 nm from the surface of the nanorod (red region in panel b). The oscillatory behavior below 5 nm suggests that the Keggin anions form discrete layers at the interface. The arrows pointing down mark the positions of concentration peaks of the Keggin anions obtained from the molecular dynamics simulation. (d) Fast Fourier transform (FFT) profiles along the $y$-direction of the image intensity for different layers of the Keggin anions (i−iv marked in panel c). The peak features suggest spatial ionic ordering along the interface. For comparison, the FFT for a region in the bulk solution is plotted (v marked in panel c), which does not show a peak feature. All curves are normalized and vertically offset. The shaded areas represent the confidence bounds of the FFT curves (one standard deviation). The arrows mark the positions of the radially averaged FFT peaks for each layer of the Keggin anions obtained from the molecular dynamics simulation.

microscope (TEM). The pH of the solution was adjusted to 1.2 ± 0.2 by hydrochloric acid (HCl) to stabilize the Keggin anions.[48] After mixing, a few microliters of the solution were applied to a lacey carbon TEM grid, and the excess liquid was blotted away from both sides with filter papers.[31] The grid was then rapidly cooled to 90 K inside liquid ethane for vitrification to occur. Finally, samples were transferred into a TEM and imaged under a low electron dose (~100 e/Å$^2$) at 100 K to reduce electron beam damage.[33] With an under-defocus of ~250 nm, we obtained adequate image contrast that resolves individual Keggin anions in the vitrified solution (see Supporting Information for details).

Figure 1b shows a representative cryo-TEM image of the interface between a positively charged nanorod and the electrolyte solution. In general, such interfaces can be divided into two characteristic regions. At the nanorod surface, the Keggin anions accumulate and form a dense and ordered structure. Beyond this dense structure, a homogeneous bulk solution appears, in which the Keggin anions are more sparsely distributed. To reveal the ionic distribution perpendicular to the interface, we integrate the image intensity along the length of the nanorod ($y$-axis), as shown in Figure 1c. The emergence of four distinct peaks along the $x$-axis indicates that the Keggin anions form four discrete layers at the interface, with an averaged separation of 1.3 nm, which is slightly larger than the diameter of a dehydrated Keggin anion (1.1 nm). The prominence of the first peak suggests that the Keggin anions are densely packed in the first layer next to the surface.

We further study the spatial ionic ordering along the interface ($y$-axis) by performing the fast Fourier transform (FFT) of the image profile for each layer of the Keggin anions. We observe an FFT peak in all of the four layers at the interface, in sharp contrast to a region in the bulk solution, which does not show an FFT peak (see Figure 1d). In particular, all of the peak positions are in the same spatial frequency range of 0.6−0.7 nm$^{-1}$, which corresponds to the spatial periodicity range of 1.4−1.7 nm. We note that such spatial periodicity along the $y$-axis is slightly larger than the averaged periodicity of 1.3 nm along the $x$-axis. This asymmetry suggests that the Keggin anions are pushed onto the surface of the nanorod because of their attractive interaction with the surface charge. In addition, the FFT peaks become broadened from the first layer to the fourth layer, indicating that the ionic distribution becomes less ordered with increasing distance from the charged surface.

The layered distribution of the Keggin anions can be generally explained as an interplay between the finite ion size, the high surface charge density, and the high ion valency. We perform molecular dynamics simulation in order to understand the ionic structure. To capture the essence of the physical mechanism, we represent the problem with a primitive model, where the solvent is described as a structureless continuum with a fixed dielectric constant, and the ions interact via electrostatic and hard-sphere interactions. The curvature of the nanorods is neglected in the simulations (see Supporting Information for details). In the simulation, the effective diameters of the Keggin ions (1.5 nm) include the first hydration shell,[49] and the monovalent counterions ($Cl^-$) are excluded. With an experimentally relevant surface charge density of 4.5 e/nm$^2$ (ref 50), the simulation shows four layers of the multivalent counterions at the planar interface (Figure 2a), while the hydronium co-ions are repelled from the layering structure (Figure S2). The simulated concentration distribution of the Keggin anions is plotted in Figure 2b. The peak positions of the concentration profile agree well with the peak positions of the integrated image intensity profile (see arrows in Figure 1c). Such an oscillatory concentration profile of multivalent counterions cannot be described by the classical mean-field Poisson−Boltzmann theory (inset of Figure 2b). In order to theoretically capture the layering behavior, the excluded volume of the ions must be considered in their chemical potential,[38] either in terms of local ionic densities or integral-weighted ionic densities,[39−43] as shown by the inset of Figure 2b.

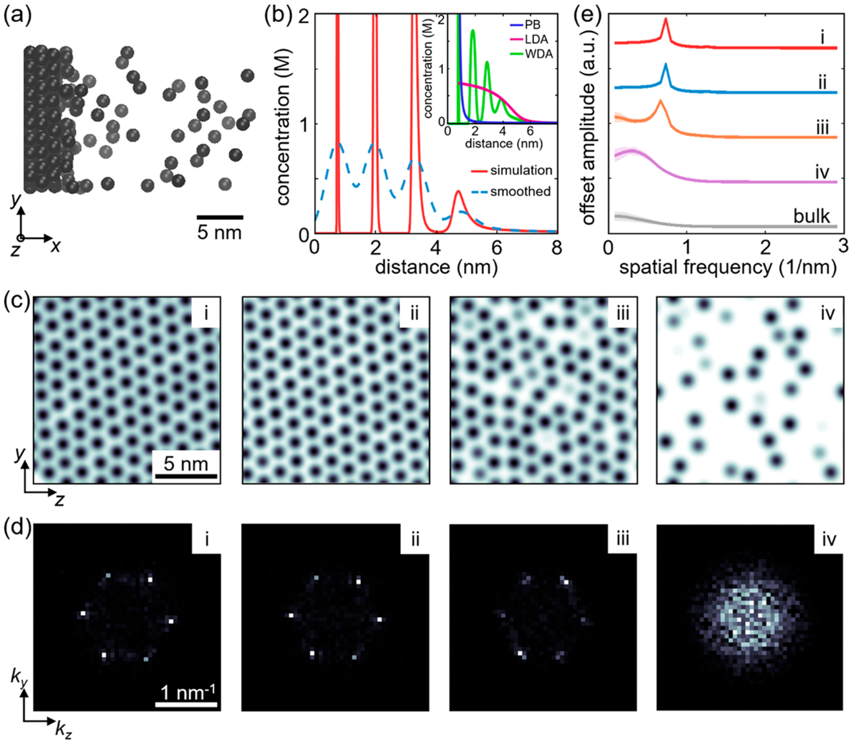

**Figure 2.** Molecular dynamics simulation of ionic distributions at the liquid−solid interface. (a) A snapshot view in the molecular dynamics simulation showing the Keggin anions form four discrete layers at the interface with a surface charge density of 4.5 e/nm$^2$. (b) Concentration distribution of the centers of the Keggin anions obtained from the simulation (solid red curve). The dashed curve shows a smoothed concentration profile (convolved with a Gaussian). The peaks of these profiles are presented as downward pointing arrows in Figure 1c. The inset shows theoretical predictions of the counterion concentration with the Poisson−Boltzmann equation (PB), weighted-density approximation (WDA), and local-density approximation (LDA). The latter two include the excluded volume effect for the counterions (see Supporting Information for details). (c) Cross-sectional snapshots (slices in the *y*−*z* plane) for each layer of the Keggin anions in the simulation. The ionic structures become less ordered from the first layer to the fourth layer. The Keggin anions are presented in space by Gaussian spheres with a variance of a half ionic radius. (d) Time-averaged two-dimensional FFT profiles of the cross-sectional slices of the ionic layers. (e) Radially averaged FFT profiles for all ionic layers. The shaded areas represent one standard deviation of the FFT curves. The peaks of these profiles are presented as down-pointing arrows in Figure 1D.

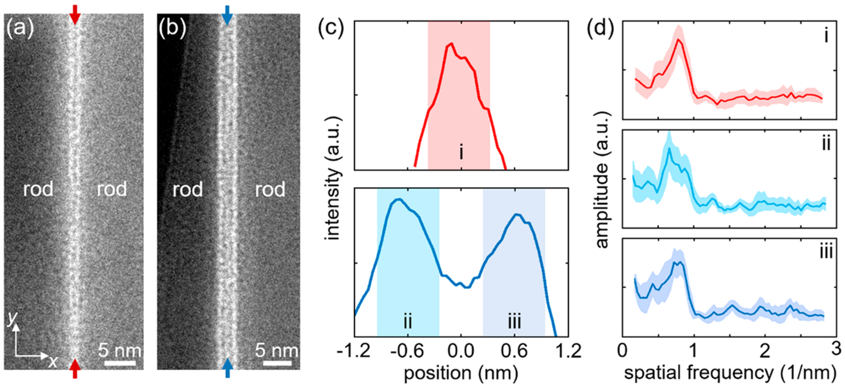

**Figure 3.** Correlated ionic structures under extreme confinement. (a, b) Cryo-TEM images of the ionic solution confined between aggregated parallel nanorods. (c) Integrated image intensity profiles of the regions between the nanorods (top, panel a; bottom, panel b). The profiles confirm that the Keggin anions form monolayer and bilayer structures with respect to different channel widths. The zero positions are marked by the arrows in panels a and b. (d) FFT profiles of the image intensity for different layers of the Keggin anions (i−iii marked in panel b). The peak features suggest the spatial ordering of the ions along the interface. All curves are normalized. The shaded areas represent the confidence bounds of the FFT curves (one standard deviation).

We now apply the simulation results to examine the ionic distributions within each layer. Because of the reduction of the electrostatic interaction with the surface, the ionic structures become less ordered from the first layer to the fourth layer, as revealed by the two-dimensional cross-sectional maps of the multivalent counterions (Figure 2c). Within the simulation size (lateral dimension 15 × 15 nm$^2$), the ionic distributions in the first two layers possess a hexagonal symmetry, as shown by the two-dimensional FFT profiles (Figure 2d). On a larger scale beyond the simulation, polycrystalline structures could emerge, and therefore, the two-dimensional FFT profiles would become isotropic. For this reason, we perform radial averaging on the two-dimensional FFTs to represent the ionic ordering along the interface for each layer of the Keggin anions (Figure 2e). The peak positions of the radially averaged FFTs agree well with the peak positions of the FFTs of the image intensity profiles (see arrows in Figure 1d). The above simulation captures the room-temperature interfacial ionic arrangements controlled by electrostatic and excluded volume interactions, supporting the main observations from our cryo-TEM imaging.

The cryo-imaging technique also allows us to visualize ionic distributions under confinement. In the solution, the multivalent anions mediate an "anomalous" attraction between the positively charged surfaces (so-called like-charge attraction),[16,51] which leads to aggregation of the nanorods (Figure S3). Such aggregation gives rise to extreme confinement of the electrolyte solution, as shown by the cryo-TEM images in Figure 3a,b. With different confinement widths of 1.3 and 2.5 nm, the Keggin anions form monolayer and bilayer structures between the parallel nanorods, as confirmed by the integrated image intensity profiles in Figure 3c. A variation of the number of layers is also observed in unconfined configuration (Figure S4), suggesting a variation of surface charge density in the sample. The FFT profiles of the image intensity for each layer are plotted in Figure 3d. For all layers, an FFT peak emerges in the spatial frequency range 0.7−0.8 $\text{nm}^{-1}$, corresponding to a spatial periodicity of 1.2−1.4 nm. The observed monolayer and bilayer correlated ionic structures resemble a series of repulsively interacting systems under confinement, such as colloids[52] and dusty plasmas.[53]

In cryo-TEM, the sensitivity of vitrified water to an electron beam restricts the electron dose to ∼100 e/$\text{Å}^2$, which limits the imaging spatial resolution by electron shot noise.[54] On the basis of the signal-to-noise analysis of our experiment with Keggin ions, we estimate that the smallest diameter of a heavy metal particle that can be resolved is ∼0.7 nm (Figure S5). In biological samples, this limitation can be overcome by aligning and averaging numerous low dose images of highly similar biomolecules. Such an averaging method has resolved individual monatomic ions that bind to biological channels.[55,56]

Another question regarding cryo-TEM is whether the vitrification preserves the intrinsic ionic arrangements. From a macroscopic view of heat and mass transfer, the thermal diffusivities in gold and water are over 2 orders of magnitude higher than the ion diffusivity in water, suggesting that freezing occurs much faster than ionic motion. This is supported by the homogeneity of vitrified ionic solutions, which are supersaturated at cryogenic temperatures[37] (Figure S6). Moreover, based on previous research in biology, molecular structures can be preserved by vitrification down to the atomic scale.[31−34] This fact is consistent with the compatibility between our experimental observation and the theoretical description of room-temperature electrical double layers.

In conclusion, we have presented, for the first time, cryo-TEM images of discrete counterions in electrical double layers. The distribution of the multivalent Keggin anions at the highly charged surface exhibits discrete layering and strong three-dimensional ordering. The utility of cryo-TEM provides new opportunities to explore the liquid−solid interfaces at the single-ion level. Furthermore, it offers a mechanism to validate and improve theoretical models. Finally, the ability to resolve ionic structures under extreme confinement provides a new route to explore nanofluidic devices and nanostructured electrochemical materials.

## ■ ASSOCIATED CONTENT

### Supporting Information

The Supporting Information is available free of charge at https://pubs.acs.org/doi/10.1021/acs.nanolett.0c02669.

> Sample preparation; cryo-TEM imaging method and signal-to-noise analysis; molecular dynamics simulation; continuum theories; aggregation of amine-functionalized nanorods (PDF)

## ■ AUTHOR INFORMATION

### Corresponding Author

**Arun Majumdar** − *Department of Mechanical Engineering and Precourt Institute for Energy, Stanford University, Stanford, California 94305, United States; Department of Photon Science, SLAC National Accelerator Laboratory, Menlo Park, California 94025, United States;* orcid.org/0000-0003-4226-9705; Email: amajumdar@stanford.edu

### Authors

**Hao-Kun Li** − *Department of Mechanical Engineering, Stanford University, Stanford, California 94305, United States*

**J. Pedro de Souza** − *Department of Chemical Engineering, Massachusetts Institute of Technology, Cambridge, Massachusetts 02139, United States*

**Ze Zhang** − *Department of Mechanical Engineering, Stanford University, Stanford, California 94305, United States;* orcid.org/0000-0002-3019-0138

**Joel Martis** − *Department of Mechanical Engineering, Stanford University, Stanford, California 94305, United States*

**Kyle Sendgikoski** − *Department of Materials Science and Engineering and Department of Physics, University of Maryland, College Park, Maryland 20742, United States*

**John Cumings** − *Department of Materials Science and Engineering, University of Maryland, College Park, Maryland 20742, United States*

**Martin Z. Bazant** − *Department of Chemical Engineering and Department of Mathematics, Massachusetts Institute of Technology, Cambridge, Massachusetts 02139, United States;* orcid.org/0000-0002-8200-4501

Complete contact information is available at: https://pubs.acs.org/10.1021/acs.nanolett.0c02669

### Author Contributions

H.-K.L., Z.Z, J.C., and A.M. conceived the project. H.-K.L. conducted the experiments. Z.Z., J.M., K.S., and J.C. assisted the experiments. J.P.D. and M.B. performed the theoretical analysis. H.-K.L., J.P.D., and A.M. wrote the manuscript with inputs from all authors. H.-K.L. and J.P.D. contributed equally to this work.

### Notes

The authors declare no competing financial interest.

## ■ ACKNOWLEDGMENTS

The authors thank A. Noy, Y. Cui, and Z. Siwy for helpful discussions. We also thank L. Montabana, D.-H. Chen and W. Chiu at Stanford and SLAC, as well as W.-A. Chiou in the Maryland NanoCenter for facilitating cryo-EM training. This work was supported as part of the Center for Enhanced Nanofluidic Transport (CENT), an Energy Frontier Research

Center funded by the U.S. Department of Energy, Office of Science, Basic Energy Sciences under Award no. DE-SC0019112. Z.Z. and J.M. acknowledge financial support by the Air Force Office Scientific Research under grant no. FA9550-19-1-0309. J.P.D. acknowledges support from the National Science Foundation Graduate Research Fellowship under award number no. 1122374. The cryo-TEM imaging was performed at the Stanford-SLAC Cryo-EM Facility. Part of the work was performed at the Stanford Nano Shared Facilities (SNSF) and supported by the National Science Foundation under award ECCS-1542152. K3IS camera and support are courtesy of Gatan.

## ■ REFERENCES

(1) Hückel, E.; Debye, P. The theory of electrolytes: I. lowering of freezing point and related phenomena. *Phys. Z.* **1923**, *24*, 185−206.

(2) Israelachvili, J. N. *Intermolecular and surface forces*; Academic Press: New York, 2015.

(3) Lyklema, J. *Fundamentals of interface and colloid science: solid liquid interfaces*; Academic Press: London, 1995.

(4) Bloomfield, V. A. DNA condensation by multivalent cations. *Biopolymers* **1997**, *44*, 269−282.

(5) Schoch, R. B.; Han, J.; Renaud, P. Transport phenomena in nanofluidics. *Rev. Mod. Phys.* **2008**, *80*, 839−883.

(6) Bocquet, L.; Charlaix, E. Nanofluidics, from bulk to interfaces. *Chem. Soc. Rev.* **2010**, *39*, 1073−1095.

(7) Werber, J. R.; Osuji, C. O.; Elimelech, M. Materials for next-generation desalination and water purification membranes. *Nat. Rev. Mater.* **2016**, *1*, 1−15.

(8) González, A.; Goikolea, E.; Barrena, J. A.; Mysyk, R. Review on supercapacitors: technologies and materials. *Renewable Sustainable Energy Rev.* **2016**, *58*, 1189−1206.

(9) Park, M.; Ryu, J.; Wang, W.; Cho, J. Material design and engineering of next-generation flow-battery technologies. *Nat. Rev. Mater.* **2017**, *2*, 1−18.

(10) Choi, N. S.; Chen, Z.; Freunberger, S. A.; Ji, X.; Sun, Y. K.; Amine, K.; Yushin, G.; Nazar, L. F.; Cho, J.; Bruce, P. G. Challenges facing lithium batteries and electrical double-layer. *Angew. Chem., Int. Ed.* **2012**, *51*, 9994−10024.

(11) Vayenas, C. G.; Brosda, S.; Pliangos, C. The double-layer approach to promotion, electrocatalysis, electrochemical promotion, and metal−support interactions. *J. Catal.* **2003**, *216*, 487−504.

(12) Grosberg, A. Y.; Nguyen, T. T.; Shklovskii, B. I. Colloquium: the physics of charge inversion in chemical and biological systems. *Rev. Mod. Phys.* **2002**, *74*, 329−345.

(13) Kilic, M. S.; Bazant, M. Z.; Ajdari, A. Steric effects in the dynamics of electrolytes at large applied voltages. I. Double-layer charging. *Phys. Rev. E* **2007**, *75*, 021502.

(14) Bazant, M. Z.; Storey, B. D.; Kornyshev, A. A. Double layer in ionic liquids: Overscreening versus crowding. *Phys. Rev. Lett.* **2011**, *106*, 046102.

(15) Kornyshev, A. A.; Qiao, R. Three-dimensional double layers. *J. Phys. Chem. C* **2014**, *118* (32), 18285−18290.

(16) Šamaj, L.; Trizac, E. Wigner-crystal formulation of strong-coupling theory for counterions near planar charged interfaces. *Phys. Rev. E* **2011**, *84*, 041401.

(17) Fedorov, M. V.; Kornyshev, A. A. Ionic liquids at electrified interfaces. *Chem. Rev.* **2014**, *114*, 2978−3036.

(18) Righini, R. Ultrafast Optical Kerr-Effect in Liquids and Solids. *Science* **1993**, *262*, 1386−1390.

(19) Miranda, P. B.; Shen, Y. R. Liquid interfaces: A study by sum-frequency vibrational spectroscopy. *J. Phys. Chem. B* **1999**, *103*, 3292.

(20) Bouzigues, C. I.; Tabeling, P.; Bocquet, L. Nanofluidics in the Debye layer at hydrophilic and hydrophobic surfaces. *Phys. Rev. Lett.* **2008**, *101*, 114503.

(21) Andanson, J. M.; Baiker, A. Exploring catalytic solid/liquid interfaces by in situ attenuated total reflection infrared spectroscopy. *Chem. Soc. Rev.* **2010**, *39*, 4571−4584.

(22) Chu, M.; Miller, M.; Dutta, P. Crowding and anomalous capacitance at an Electrode−Ionic liquid interface observed using operando x-ray scattering. *ACS Cent. Sci.* **2016**, *2*, 175−180.

(23) Favaro, M.; Jeong, B.; Ross, P. N.; Yano, J.; Hussain, Z.; Liu, Z.; Crumlin, E. J. Unravelling the electrochemical double layer by direct probing of the solid/liquid interface. *Nat. Commun.* **2016**, *7*, 1−8.

(24) Israelachvili, J. N.; Pashley, R. M. Molecular layering of water at surfaces and origin of repulsive hydration forces. *Nature* **1983**, *306*, 249−250.

(25) Bailo, E.; Deckert, V. Tip-enhanced Raman scattering. *Chem. Soc. Rev.* **2008**, *37*, 921−930.

(26) Amemiya, S.; Bard, A. J.; Fan, F. R. F.; Mirkin, M. V.; Unwin, P. R. Scanning electrochemical microscopy. *Annu. Rev. Anal. Chem.* **2008**, *1*, 95−131.

(27) Chen, C. C.; Zhou, Y.; Baker, L. A. Scanning ion conductance microscopy. *Annu. Rev. Anal. Chem.* **2012**, *5*, 207−228.

(28) Ricci, M.; Spijker, P.; Voïtchovsky, K. Water-induced correlation between single ions imaged at the solid−liquid interface. *Nat. Commun.* **2014**, *5*, 1−8.

(29) Fukuma, T.; Garcia, R. Atomic-and Molecular-resolution mapping of solid−liquid interfaces by 3D atomic force microscopy. *ACS Nano* **2018**, *12*, 11785−11797.

(30) Mao, X.; Brown, P.; Cervinka, C.; Hazell, G.; Li, H.; Ren, Y.; Chen, D.; Atkin, R.; Eastoe, J.; Grillo, I.; Padua, A.. A. H.; Costa Gomes, M.. F.; Hatton, T. A. Self-assembled nanostructures in ionic liquids facilitate charge storage at electrified interfaces. *Nat. Mater.* **2019**, *18*, 1350−1357.

(31) Dubochet, J.; Adrian, M.; Chang, J. J.; Homo, J. C.; Lepault, J.; McDowall, A. W.; Schultz, P. Cryo-electron microscopy of vitrified specimens. *Q. Rev. Biophys.* **1988**, *21*, 129−228.

(32) Dubochet, J. The physics of rapid cooling and its implications for cryoimmobilization of cells. *Methods Cell Biol.* **2007**, *79*, 7−21.

(33) Henderson, R. Overview and future of single particle electron cryomicroscopy. *Arch. Biochem. Biophys.* **2015**, *581*, 19−24.

(34) Fernandez-Leiro, R.; Scheres, S. H. Unravelling biological macromolecules with cryo-electron microscopy. *Nature* **2016**, *537*, 339−346.

(35) Neyman, A.; Meshi, L.; Zeiri, L.; Weinstock, I. A. Direct imaging of the ligand monolayer on an anion-protected metal nanoparticle through cryogenic trapping of its solution-state structure. *J. Am. Chem. Soc.* **2008**, *130*, 16480−16481.

(36) Wang, Y.; Zeiri, O.; Raula, M.; Le Ouay, B.; Stellacci, F.; Weinstock, I. A. Host−guest chemistry with water-soluble gold nanoparticle supraspheres. *Nat. Nanotechnol.* **2017**, *12*, 170.

(37) Schreiber, R. E.; Houben, L.; Wolf, S. G.; Leitus, G.; Lang, Z. L.; Carbó, J. J.; Poblet, J. M.; Neumann, R. Real-time molecular scale observation of crystal formation. *Nat. Chem.* **2017**, *9*, 369−373.

(38) Borukhov, I.; Andelman, D.; Orland, H. Steric effects in electrolytes: A modified Poisson-Boltzmann equation. *Phys. Rev. Lett.* **1997**, *79*, 435.

(39) Tarazona, P.; Evans, R. A simple density functional theory for inhomogeneous liquids: Wetting by gas at a solid-liquid interface. *Mol. Phys.* **1984**, *52*, 847−857.

(40) Bazant, M. Z.; Kilic, M. S.; Storey, B.; Ajdari, A. Towards an understanding of induced-charge electrokinetics at large applied voltages. *Adv. Colloid Interface Sci.* **2009**, *152*, 48−88.

(41) Roth, R. Fundamental measure theory for hard-sphere mixtures: a review. *J. Phys.: Condens. Matter* **2010**, *22*, 063102.

(42) Giera, B.; Henson, N.; Kober, E. M.; Shell, M. S.; Squires, T. M. Electric double-layer structure in primitive model electrolytes: comparing molecular dynamics with local-density approximations. *Langmuir* **2015**, *31*, 3553−3562.

(43) de Souza, J. P.; Goodwin, Z. A. H.; McEldrew, M.; Kornyshev, A. A.; Bazant, M. Z. Interfacial layering in the electrical double layer of ionic liquids. *Phys. Rev. Lett.* **2020**, *125*, 116001.

(44) Shapovalov, V. L.; Brezesinski, G. Breakdown of the Gouy−Chapman model for highly charged Langmuir monolayers: counterion size effect. *J. Phys. Chem. B* **2006**, *110*, 10032−10040.

(45) Biesheuvel, P. M.; Van Soestbergen, M. Counterion volume effects in mixed electrical double layers. *J. Colloid Interface Sci.* **2007**, *316*, 490−499.

(46) Mezger, M.; Schroder, H.; Reichert, H.; Schramm, S.; Okasinski, J. S.; Schoder, S.; Honkimaki, V.; Deutsch, M.; Ocko, B. M.; Ralston, J.; Rohwerder, M.; Stratmann, M.; Dosch, H. Molecular layering of fluorinated ionic liquids at a charged sapphire (0001) surface. *Science* **2008**, *322*, 424−428.

(47) Misra, A.; Kozma, K.; Streb, C.; Nyman, M. Beyond charge balance: counter-cations in polyoxometalate chemistry. *Angew. Chem., Int. Ed.* **2020**, *59*, 596−612.

(48) Zhu, Z.; Tain, R.; Rhodes, C. A study of the decomposition behaviour of 12-tungstophosphate heteropolyacid in solution. *Can. J. Chem.* **2003**, *81*, 1044−1050.

(49) Lopez, X.; Nieto-Draghi, C.; Bo, C.; Avalos, J. B.; Poblet, J. M. Polyoxometalates in solution: molecular dynamics simulations on the $\alpha$-$PW_{12}O_{40}^{3-}$ Keggin anion in aqueous media. *J. Phys. Chem. A* **2005**, *109*, 1216−1222.

(50) Dubois, L. H.; Nuzzo, R. G. Synthesis, structure, and properties of model organic surfaces. *Annu. Rev. Phys. Chem.* **1992**, *43*, 437−463.

(51) Misra, R. P.; de Souza, J. P.; Blankschtein, D.; Bazant, M. Z. Theory of Surface Forces in Multivalent Electrolytes. *Langmuir* **2019**, *35*, 11550−11565.

(52) Neser, S.; Bechinger, C.; Leiderer, P.; Palberg, T. Finite-size effects on the closest packing of hard spheres. *Phys. Rev. Lett.* **1997**, *79*, 2348.

(53) Teng, L. W.; Tu, P. S.; Lin, I. Microscopic observation of confinement-induced layering and slow dynamics of dusty-plasma liquids in narrow channels. *Phys. Rev. Lett.* **2003**, *90*, 245004.

(54) de Jonge, N. Theory of the spatial resolution of (scanning) transmission electron microscopy in liquid water or ice layers. *Ultramicroscopy* **2018**, *187*, 113−125.

(55) Tao, X.; Hite, R. K.; MacKinnon, R. Cryo-EM structure of the open high-conductance $Ca^{2+}$-activated $K^+$ channel. *Nature* **2017**, *541*, 46−51.

(56) Liu, S.; Chang, S.; Han, B.; Xu, L.; Zhang, M.; Zhao, C.; Yang, W.; Wang, F.; Li, J.; Delpire, E.; Ye, S.; Bai, X.-c.; Guo, J. Cryo-EM structures of the human cation-chloride cotransporter KCC1. *Science* **2019**, *366*, 505−508.